

# Ion Optics for Laboratory Spacecraft Wake Generation

Kaylee Champion<sup>1</sup>, and Hanspeter Schaub<sup>2</sup>

*Department of Aerospace Engineering Sciences, University of Colorado Boulder, Boulder, Colorado*

**Abstract**—Novel active and passive touchless potential sensing techniques have been investigated in the Geosynchronous and cislunar region. These methods involve utilizing an electron gun to emit secondary electron and x-ray emissions. Cislunar spacecraft may be mesothermal with respect to the plasma, thus generating spacecraft wake formations, which have unknown impacts on touchless potential sensing. Wakes may be generated in the ECLIPS vacuum chamber at the University of Colorado Boulder to determine how the wake formations should be accounted for or taken advantage of. However, the ion beam generated from a commercial off-the-shelf device is smaller than required. Further, the emitted beam expands radially outward. To correct this, electrostatic lenses have been designed to expand the ion emission to encompass a test object and refocus the ion beam to simulate a radially non-expanding ion flow. The installation and characterization of these lenses are presented, and preliminary simulations of the ion wake experiment are shown. The experimental and numerical simulations show good agreement, enabling the installation of simple electrostatic lenses for ion beam manipulation in vacuum systems.

## I. MOTIVATION AND BACKGROUND

Novel active potential sensing methods have been investigated for application in the Geosynchronous region (GEO) [1–4]. Active potential sensing involves a servicing spacecraft directing an electron beam at a target so that secondary electrons [5, 6] and x-rays [7, 8] are emitted from the surface. The use of a vacuum ultraviolet laser has also been investigated as a method to excite photoemissions from a target [9]. The incoming signals are then measured, and the servicer utilizes the measurements to infer the potential of the target with respect to its own potential. This potential measurement may be used to avoid electrostatic discharges during docking procedures, account for perturbing electrostatic torques during proximity operations, and provide a step towards electrostatic actuation. Electrostatic actuation can be used to detumble or reorbit uncooperative targets, dock to incoming bodies, and conduct touchless in-situ servicing [8, 10, 11]. As more missions are designated for cislunar space, this technology may be expanded there as well. However, the complexity of the cislunar environment presents novel challenges for touchless potential sensing.

When a spacecraft travels through plasma, the impacting electrons and ions are disturbed and pushed out of the way,

<sup>1</sup>: Graduate Research Assistant, Ann and H.J. Smead Department of Aerospace Engineering Sciences, Colorado Center for Astrodynamic Research (email: kaylee.champion@colorado.edu)

<sup>2</sup>: Professor and Department Chair, Schaden Leadership Chair, Ann and H.J. Smead Department of Aerospace Engineering Sciences, Colorado Center for Astrodynamic Research. AAS Fellow, AIAA Fellow

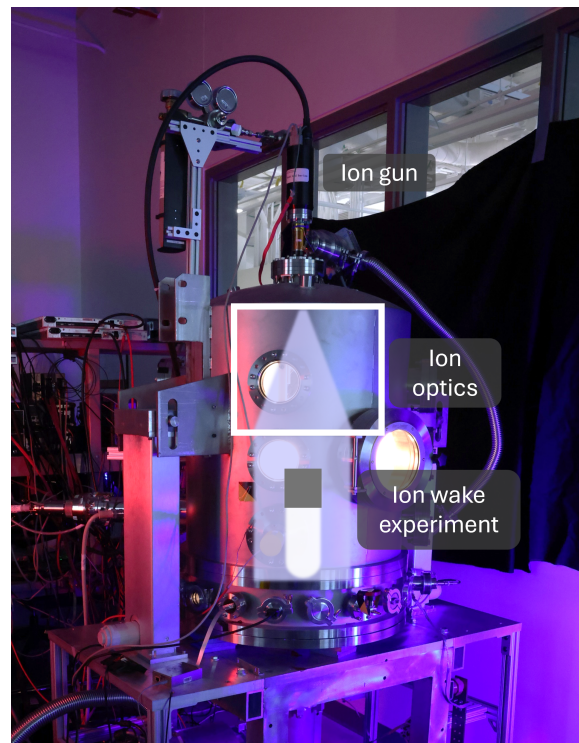


**Fig. 1:** Proposed ion wake experimental implementation in the ECLIPS vacuum chamber

similar to how an airplane or boat pushes air or water aside, respectively, as it travels. In hot plasma environments, the ions and electrons are capable of catching back up to the spacecraft and continuing to impact on all sides. In less energetic plasma environments, the thermal velocity of the ions is less than the velocity of the spacecraft, meaning the spacecraft is mesothermal with respect to the plasma ( $v_i < v_{sc} < v_e$ ). It should be noted that this is the velocity of the spacecraft with respect to the plasma, or the velocity of the spacecraft minus the bulk flow of the plasma. In these conditions, it may take several spacecraft lengths for the ions to catch back up, leaving a complex ion void region on the anti-velocity side of the spacecraft and a high density ion region on the ram side [12]. This results in varying plasma and potential field conditions around the spacecraft. Spacecraft wakes do not occur in GEO, and their impacts on sensing in cislunar space have not yet been explored.

Numerical programs, such as NASCAP-2k and SPIS, can be utilized to investigate spacecraft-plasma interactions and

electron emissions. However, these programs include assumptions about the space environment and interactions that may not properly capture the actual conditions. For example, the electron emissions or electron beam may follow different trajectories in different regions of the wake, or small changes in the potential field due to the wake may not be captured in simulations. Therefore, it is desirable to complement numerical simulations with experimental results to validate the modeled behavior acceptably represents realistic scenarios. This study focuses on enabling spacecraft wake generation in the Electrostatic Charging Laboratory for Interactions between Plasma and Spacecraft (ECLIPS) vacuum chamber located at the Autonomous Vehicles Systems (AVS) Laboratory at the University of Colorado Boulder.

Spacecraft wake experiments have been extensively conducted to broaden our understanding of the wake phenomena and its impact on spacecraft missions. Several laboratory experiments have helped determine properties of a spacecraft wake [13–17], characterize how wake formation may alter space plasma measurements [18, 19], and even investigate how cislunar wakes impact lunar regolith charging [20]. These experiments involve an ion source, an object to obstruct the flow of plasma, and sensors such as Langmuir probes and Faraday cups to determine the property of the plasma. It would be straightforward to implement a similar setup in the ECLIPS vacuum chamber. However, the 1402 Ion Gun from Non Sequitur Technologies installed in the ECLIPS chamber emits a narrow, expanding ion beam that may not be sufficient to fully surround an object and generate an ion wake. In addition, the beam expands radially outwards throughout the length of the chamber, which does not represent the parallel flow expected from cislunar plasma. To ameliorate this limitation, charged particle optics are utilized to expand and refocus the beam such that measurable wakes may be generated, as shown in Fig. 1. Charged particle optics involves manipulating the trajectory of charged particles by altering the ambient electric or magnetic field and has been a topic of study since the early 20th century, with several publications outlining the general concepts [21–24]. Altering charged particle trajectories has been used to focus ion beams for mass spectrometry [25, 26], radiotherapy for cancer patients [27], sample etching and preparation [28, 29], investigating irradiation effects on materials [30, 31], and more. This study aims to expand this research by using charged particle optics to enable wake experiments. The results could also be extended to any experiment in which it is beneficial to expand the installed ion gun’s capability to manipulate the ion beam.

For low energy ion beams (5 eV to 50 keV), electrostatic lenses are generally more efficient than magnetic lenses [22]. Furthermore, implementing simple electrostatic lenses allows for easy adaptability and implementation in other vacuum systems. Accordingly, electrostatic lenses held at constant potentials are utilized to manipulate the ion beam.

A review of the electrostatic lens design and relevant equations are presented in Section II, the lens installation, sensor package design, and configuration of the numerical model is presented in Section III, the experiment results are discussed in Section IV, and numerical investigations into experimental

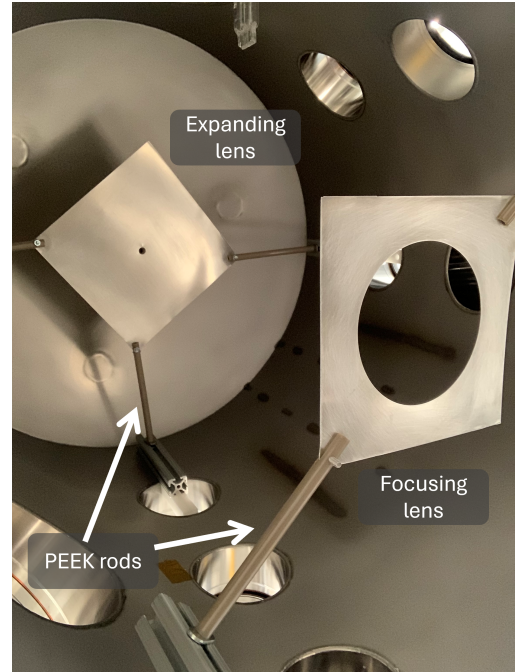


**Fig. 2:** Lens setup in the ECLIPS vacuum chamber

wake formations are shown in Section V. Last, Section VI provides an overview of the project and conclusions.

## II. ION OPTICS DESIGN

Previous work was conducted to optimize the design of the electrostatic lenses for the ECLIPS chamber [32, 33], and an overview of key takeaways and the final design is presented here.

### A. Cislunar Plasma Experimental Representation

The wake experiment is limited by experimental volume available in the ECLIPS chamber, which has a height of approximately 86 cm and a diameter of approximately 60 cm. In order to leave sufficient room for experiments to be conducted, the ion lenses are located in the top 50 cm of the chamber. Despite the size of the ECLIPS chamber, large scale phenomenon may still be represented. A scaling law can be applied to relate the spacecraft’s experimental radius  $R_0$  to the radius in the environment of interest  $R_{sim}$  [34]

$$R_{sim} = \sqrt{\frac{n_i}{n_{sim}}} R_0, \quad (1)$$

where  $n_i$  is the experiment plasma density and  $n_{sim}$  is the environment plasma density. In other words, if the density of the experimental ion beam is larger than the environmental plasma density, the experimental object represents a larger spacecraft. This relationship is derived for LEO plasma-body interactions, but it applies to processes governed by the Vlasov-Maxwell equations [34]. Thus, this may be applied to cislunar plasma environments where spacecraft wakes form. The density of the ions in the ECLIPS chamber is [32]

$$n_i = \frac{I_{beam}}{q_e A v} = \frac{I_{beam}}{q_e \pi r^2} \sqrt{\frac{m_i}{2E}}, \quad (2)$$

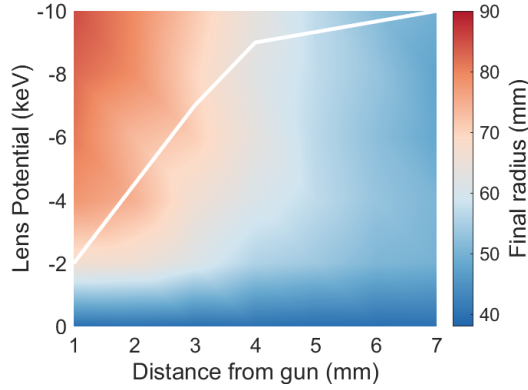


**Fig. 3:** Expected beam radius 46 cm from ion gun exit (RPA location) versus expanding lens potential and distance from ion gun. The white line indicates the voltage and distance combination at which arcing may occur.

where  $I_{\text{beam}}$  is ion gun current,  $q_e$  is the elementary charge in Coulombs,  $A$  is the final area of the beam, or  $\pi r^2$ ,  $v$  is the velocity of the ions,  $m_i$  is the mass of the ions, and  $E$  is the energy of the ions, found as  $E = 1/2 m_i v^2$ .

The argon ions ( $\text{Ar}^+$ ) generated in the ECLIPS chamber are not representative of cislunar plasma environments, which are comprised mostly of Hydrogen ions ( $\text{H}^+$ ). Fortunately, there is another scaling law that may be used to relate the velocity of two different ion species

$$v_{\text{sim}} = \sqrt{\frac{m_i}{m_{\text{sim}}}} v, \quad (3)$$

where  $v_{\text{sim}}$  is the velocity of the environment being simulated and  $m_{\text{sim}}$  is the mass of the ions in the simulated environment. Spacecraft wakes form in the cislunar Magnetosheath and Solar wind regions, which have  $\text{H}^+$  bulk velocities from 350 to 930 km/s [35]. Hydrogen ions with a bulk velocity of 400 km/s may reasonably represent solar wind or magnetosheath conditions, which corresponds to  $\text{Ar}^+$  ions with a velocity of 63.6 km/s, or a beam energy  $E_B$  of 835 eV. The beam is held at this energy in all simulations and experiments.

### B. Lens Design

SIMION, a particle tracing software package used to calculate electric fields and trajectories of charged particles, is used to design and investigate the electrostatic lenses. SIMION computes the trajectory of each charged particle from Newton's second law

$$\frac{d\mathbf{v}}{dt} = \frac{q}{m} \mathbf{E}, \quad (4)$$

where  $\mathbf{v}$ ,  $q$ , and  $m$  are respectively the particle velocity, charge, and mass,  $\mathbf{E}$  is the electric field, and  $t$  is the time. The electric field is derived from the electrostatic potential field  $V$  as

$$\mathbf{E} = -\nabla V, \quad (5)$$

while  $V$  is computed by solving Laplace's equation

$$\nabla^2 V = 0 \quad (6)$$

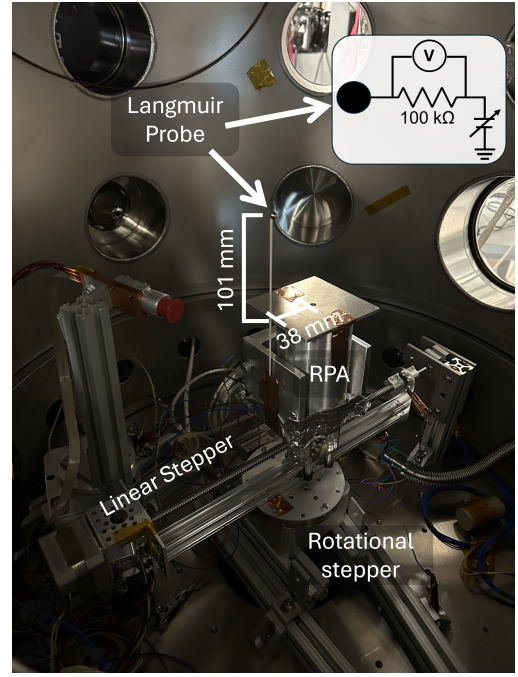


**Fig. 4:** Sensor package and Langmuir probe circuit

in the simulation domain. SIMION employs a regular Cartesian mesh with boundary conditions determined by set potentials of each electrode (Dirichlet) or by the zero-derivative of the  $V$  (Neumann). The grounded vacuum chamber wall is modeled and utilized as a 0V Dirichlet boundary.

The optimal design found in [33] utilizes two thin lenses to expand and refocus the ion gun. These lenses are simply composed of a sheet of conductive material with a hole in the middle to allow the ion beam to pass through. The lens closest to the ion gun is referred to as the expanding lens, as it is biased negatively to “pull” the ions out and expand the beam. The following lens is referred to as the focusing lens, as it is biased positively with respect to the expanding lens to stop the expansion of the beam and refocus it such that the ions flow parallel to the chamber walls. It is found that in this setup, it is ideal for the expanding lens to be as close as possible to the ion gun to generate the largest increase in beam radius. This is further described in Section III. The beam should then be allowed to expand for as long as possible before it is refocused by the focusing lens.

## III. EXPERIMENTAL SETUP

### A. Lens Setup

The lenses are constructed from 6 mm thick sheets of aluminum and held at the desired potentials using Matsusada AU-30R1 High-Voltage Power Supplies (HVPS). PEEK rods are used to electrically isolate the lenses from the chamber walls and hold them in place, as shown in Fig. 2. The ion gun outlet has a radius of 4 mm, so the radius of the focusing lens opening is 5 mm to ensure the emitted ions are not impacted. As mentioned, previous work has shown that the closer the lens is to the ion gun, the larger the final radius of the beam [33]. However, the high voltage lens may arc with

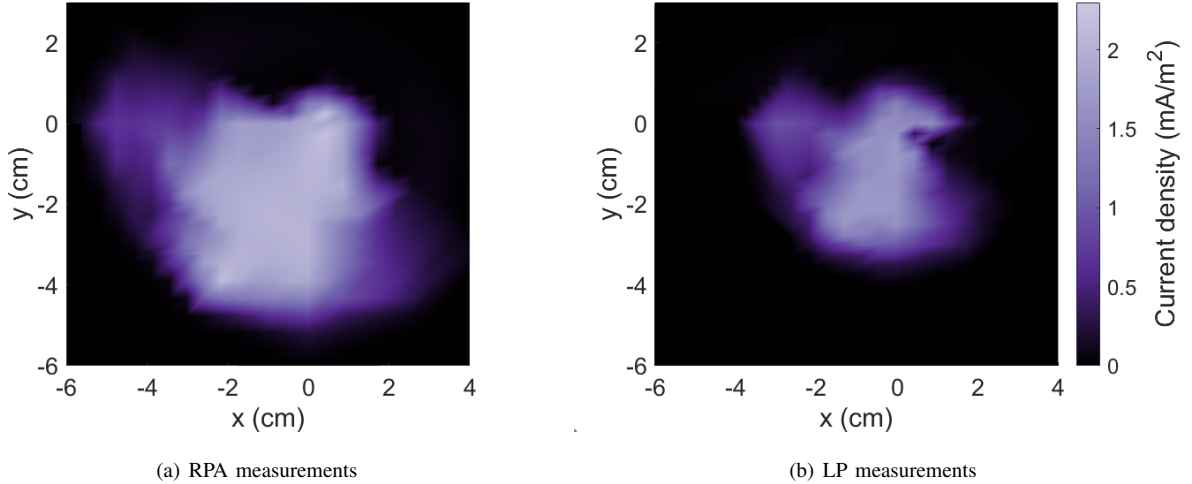


**Fig. 5:** Current density map of the unaltered ion gun emissions measured by the RPA and Langmuir Probe

the nearby, grounded ion gun. If arcing occurs, the HVPS will shut of and the ion gun may be damaged. To prevent this, the maximum voltage that can be achieved before arcing is characterized at several separation distances. To do this, two conductive sheets of aluminum are held at the desired position. One sheet is grounded, and the voltage on the second sheet is increased until arcing occurs. The arcing potential is then recorded, the separation distance is increased, and the experiment is repeated. The wake experiment is conducted in vacuum, but the arcing voltage versus separation distance is recorded in atmosphere, which is approximately 630 Torr at room temperature in Boulder, Colorado. This is done because the objects may arc through the flowing argon, resulting in lower possible potentials at a set separation distance than expected in vacuum. The arcing voltage versus separation distance is plotted as a white line over the expected final beam radius versus lens distance from the ion gun and lens potential in Fig. 3. This line indicates where the lens may be expected to arc with the ion gun, and safe lens voltage and distance combinations are located below the white line. It is evident from the figure that the largest beam radius is limited to 60 to 70 mm for a lens located 3 to 5 mm from the ion gun. The results presented in this paper are for a distance of 5 mm from the ion gun, as this allows for a large range of lens potentials to be safely tested and compared to SIMION results. The expanding lens is then set up by aligning the opening with the ion gun exit, and a level is utilized to ensure the lens is as flat as possible.

The focusing lens is placed 36 cm down from the ion gun exit because this leaves space for the experimental setup below the lens and allows for the beam to expand as much as possible before being telescoped. This lens has an opening of 50 mm, as the maximum beam radius found in [33] at the location of the focusing lens is 37 mm. This allows for the ions to pass through without intercepting the lens. The focusing lens is centered with respect to the vacuum chamber using a vertical laser, and a level is used to ensure it is as flat as possible.

### B. Sensor Package

A spherical Langmuir probe and Retarding Potential Analyzer (RPA) are used to take measurements of the ion beam at different positions, shown in Fig. 4. The Langmuir probe is constructed from a 2.5 mm radius aluminum sphere spot welded to nickel wire. The wire is electrically isolated and the probe is held in place with a ceramic tube. Before each experiment, the Langmuir probe is bombarded with 3 keV ions, the highest energy possible with the ion gun, and held at -1 kV to remove surface contamination. A sweep outside the ion beam is then conducted to obtain measurements of the expected noise level, or the load line  $\Delta V_{\text{noise}}$  [36]. This noise is generally two orders of magnitude smaller than the measurements obtained in the ion gun. The Langmuir probe is swept from 0 to -100 V in 10 V steps using a Matsusada AU-IR30 HVPS, and the voltage change  $\Delta V$  across a 100 k $\Omega$  resistor is measured using a Keithley DMM6500 multimeter for each applied potential  $V_{\text{applied}}$ . These measurements generate a current versus potential ( $I_{\text{ion}} - V_{\text{applied}}$ ) curve in the ion saturation region [37], which may be summed up as

$$I_{\text{ion}}(V_{\text{applied}}) = R \times [\Delta V(V_{\text{applied}}) - \Delta V_{\text{noise}}(V_{\text{applied}})], \quad (7)$$

where  $R$  is the resistance of the circuit. The multimeter has an internal resistance of 20 M $\Omega$ , which is added to the circuit resistance ( $R=20.1$  M $\Omega$ ). The Langmuir probe theory presented in [38] is implemented in MATLAB and utilized to obtain the ion density. The RPA was previously constructed from a Faraday cup with a front grounding grid followed by a biasing grid. An aluminum sheet is placed in front of the RPA's entrance to decrease the entrance aperture to a circle with a radius of 2.4 mm. This makes the RPA entrance comparable to the size of the Langmuir probe and allows for measurements to be taken in 5 mm steps. The RPA is located approximately 460 mm from the ion gun exit, and the Langmuir probe is positioned approximately 101 mm higher than the RPA, or 359 mm from the ion gun. Both instruments are placed on a linear stepper motor capable of moving the sensors  $\pm 10$  cm from

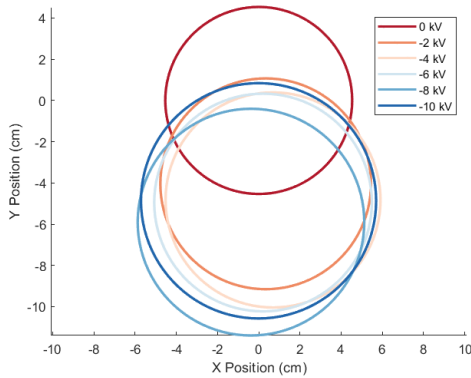


**Fig. 6:** Projections of the ion gun measurements made by the RPA for varying expanding lens potentials

the center of the chamber and a rotational stepper capable of rotating  $360^\circ$ . This allows the entire space to be characterized with a resolution of 5 mm.

### C. Configuration of SIMION Model

To determine if the ion beam is symmetrical and ensure the SIMION model is properly configured, a current density map of the ion beam is obtained, as shown in Fig. 5. As shown, the beam is not perfectly symmetric, but the highest current density region may be considered approximately circular. The beam radius is 3.84 cm as measured by the RPA and 3.15 cm as measured by the Langmuir probe. Based on this, and assuming an initial radius of 1 mm at the ion gun exit, the half angle of the beam may be estimated to be  $\approx 4.9^\circ$ .

It is interesting that the current density measured by the Langmuir probe is smaller than that measured by the RPA, as the Langmuir probe is located in a region of the beam with a smaller radius and higher current density. However, Langmuir probes are often stated to have accuracy of 20 to 50% of real values [37, 38], which may account for this discrepancy. The magnitude of the current density measured by the Langmuir probe does not change the results of this project, as the edge points of the current measurements are used to determine the size of the beam. This process is further described in Section IV-A.

## IV. RESULTS

Before combining the entire setup, the expanding and focusing lenses are individually installed and measured to test their individual effects.

### A. Expanding Lens

The expanding lens is first individually tested. Creating a detailed map of the lens, as done in Fig. 5, takes approximately four hours. In addition, it is desirable to test the entire range of lens potentials in the same sitting, as this minimizes changes to the setup or ion beam properties. Therefore, a faster method of estimating the size of the beam must be determined. The general shape of the beam is assumed to be a circle, as shown

in Section III-C. Then, at least three edge points of the beam must be found and the positions are recorded. These points are then used to find the center point of the beam  $(x_c, y_c)$  and radius  $r$  by performing a linear least squares fitting to the equation of a circle

$$r^2 = (x - x_c)^2 + (y - y_c)^2, \quad (8)$$

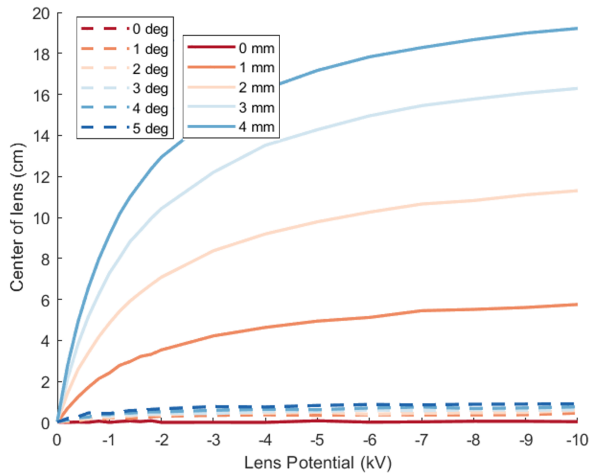
where  $x$  and  $y$  are the points in a Cartesian frame. To find these edge points, the sensors measure along the entire length of the stepper motor, then the rotational stepper motor is rotated  $90^\circ$ , and the process is repeated. This results in four edge points being recorded and utilized to determine the position and size of the circular projection of the beam. Examples of these circular projections of the beam are shown in Fig. 6.

As shown in these projections, the beam is expanded and *translated* as the potential is varied. This indicates that the lens is misaligned, meaning it is not perfectly flat or centered with respect to the ion gun. Because perfectly positioning the lens requires machine precision and is beyond the technologies available for this project, the beam translation is characterized for imperfections in beam setup.

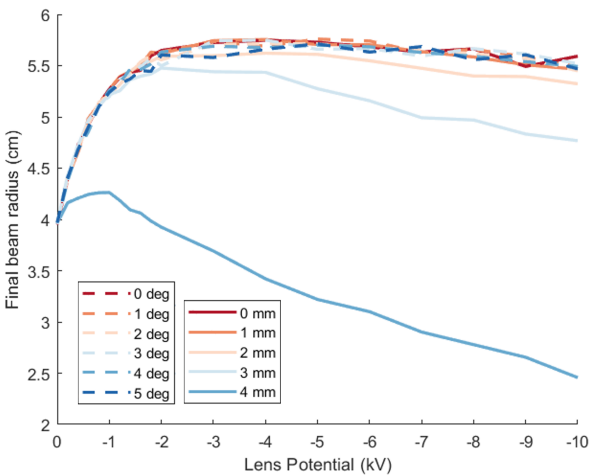
1) *Impact of Lens Misalignment:* The expanding lens is modeled in SIMION at a distance of 5 mm from the ion gun to match the experimental setup. The simulated lens is then shifted from the center of the simulation and tilted to characterize how these imperfections may impact the ion beam radii and offset. The translation, or offset, of the beam and final radius values for various beam misalignment's is shown in Fig. 7. The dashed lines display results for a perfectly centered, but tilted, beam and the solid lines represent an off-center but perfectly level lens. Interestingly, tilting the lens has a significantly smaller effect than shifting the lens with respect to the ion gun. Furthermore, a tilted lens does not seem to impact the final radius of the beam, while a lens shifted more than 2 mm has a significant impact. In general, tilting the lens appears to have negligible impact on the beam properties. Thus, any ion beam translations may be contributed to an off-center lens.

The expanding lens was set up and characterized in two separate trials. The translation of the lenses is unknown, so the recorded results are compared to SIMION results to estimate how much the lenses might be offset. The experimental and corresponding SIMION results for the two days of experiments are shown in Fig. 8. The Langmuir probe was connected to the multi-meter improperly during trial 1, so there are no Langmuir probe results for that test. It is estimated that trial 1 is offset approximately 0.9 mm and trial 2 is offset 0.5 mm. The experimental and SIMION center of beam, or magnitude of beam translation, correspond well with each other. This validates that the translation of the beam can be contributed to the lens being off-center with respect to the ion gun by sub-millimeter magnitudes. The translation due to lens misalignment may be accounted for by placing the spacecraft primitive on the stepper motor setup and moving it such that it is within the ion beam.

Interestingly, SIMION shows a quick jump in radius before a plateau, while the experimental results indicate a more gradual increase in radius and then plateau. This may be due



(a) Offset



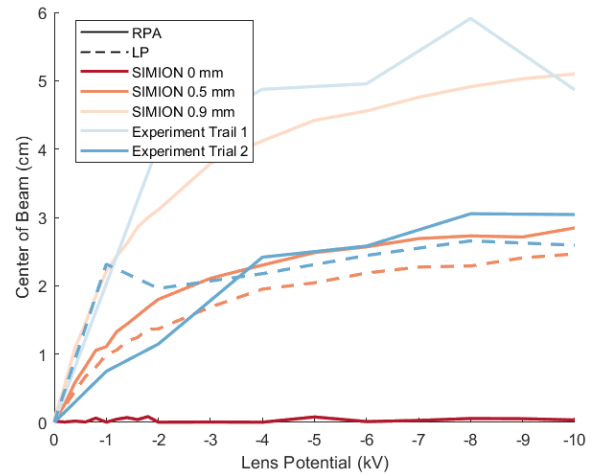
(b) Radius

**Fig. 7:** Ion beam offset (left) and radius (right) at the RPA position versus lens potential for varying misalignment's. Solid lines indicate an off-center lens and dashed indicate a tilted lens.

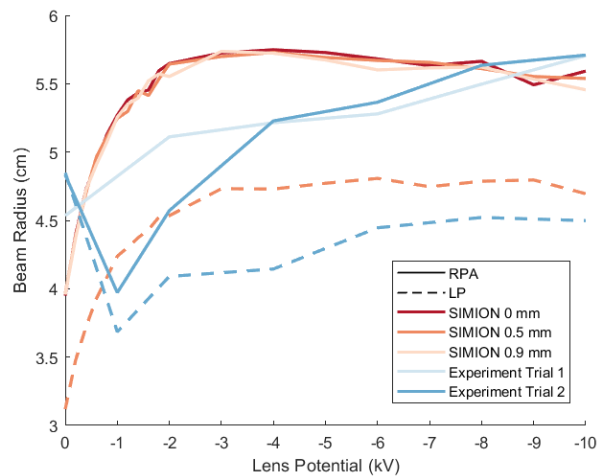
to inaccuracies in the chamber model in SIMION, as some unmodeled components such as the chamber windows or wires may slightly alter the potential fields. However, it is shown that the radius of the beam is increasing with lens potential, and the maximum radius for both appears to be approximately the same. Thus, the expanding lens is performing as designed and generating a wider beam, allowing for a larger object to be placed in the beam, or a thicker region of ions surrounding the object.

*B. Focusing Lens*

In order for the focusing lens to “compress” the ions into a smaller radius beam, the lens needs to be more positive than the preceding lens or ion source [21]. For example, if the expanding lens is set up and held at -8 keV, the focusing



(a) Offset



(b) Radius

**Fig. 8:** Ion beam offset (left) and radius (right) versus lens potential. Solid lines indicate RPA measurements, and dashed indicate Langmuir Probe measurements. Experimental data is compared to SIMION estimates of the lens misalignment. Trial 1 is estimated to be shifted 0.9 mm and Trial 2 is estimated to be shifted 0.5 mm.

lens must be more positive than -8 keV. In this scenario, the focusing lens must be positive, as the ion gun is grounded. It is found in SIMION that the beam is approximately telescoped, or the radius of the beam remains constant after the lens, when the focusing lens is at 650 V. Ideally, this would be verified experimentally by measuring the radius of the beam using the Langmuir probe and RPA. Then, the potential at which the difference between the radii is minimized may be approximated as the ideal focusing potential. Unfortunately, it is found that the proximity of the Langmuir probe to the lens significantly alters the electric field, changing the ion trajectories and RPA measurements. More specifically, the Langmuir probe attracts the ions, resulting in the RPA

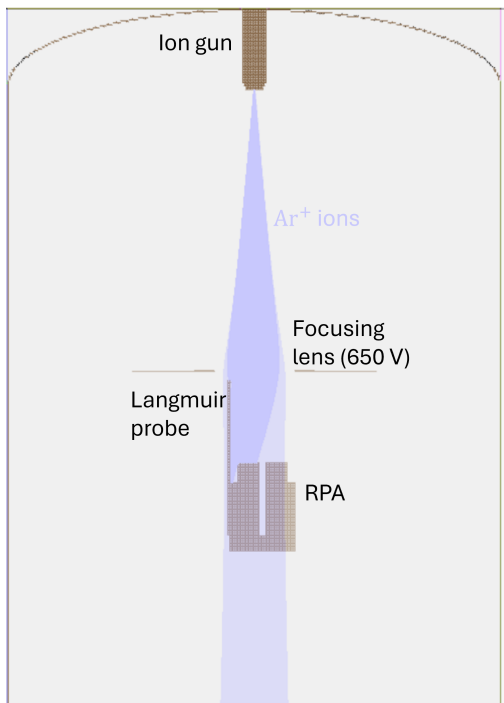


**Fig. 9:** SIMION simulation of a telescoped beam with only the focusing lens. The undisturbed beam is shown in light purple, and the beam altered by the Langmuir probe and RPA is shown in darker purple.

measuring a smaller and shifted ion beam. This behavior can be recreated in SIMION. The desired beam behavior is shown in light purple on top of the beam behavior when sensors are present in Fig. 9. In this configuration, both sensors should detect current from the beam. However, the darker purple shows how the beam is attracted towards the Langmuir probe, resulting in no current reaching the inside of the RPA. The entire setup is also modeled for the beam with just the expanding lens and no lens installed, and the Langmuir probe does not interfere with RPA measurements in these setups.

In this SIMION model, the sensor positions can be changed and the particles measured by the sensors can be recorded. This allows for the experiment to be simulated in SIMION and compared to the experimental results. During the experiments, as the beam is shrunk and deflected towards the Langmuir probe, it becomes difficult to find and record more than two points on the edge of the beam to generate a circular projection. As a result, it is simpler to compare the current densities. The Langmuir probe is located 1.6 cm below the focusing lens, so the measured beam radius and current density does not significantly vary. The average current density measured by Langmuir probe is  $1.9 \text{ mA/m}^2$  in experiments and  $2.6 \text{ mA/m}^2$  in SIMION simulations. This is a 25% difference, which is within the expected Langmuir probe measurement errors.

Because the RPA entrance is located approximately 11.6 cm from the lens, the measurements from the RPA provide the most significant insight into the changing beam behavior. The resulting measurements for varying focusing lens potentials are shown in Fig. 10. Interestingly, the measurements made by

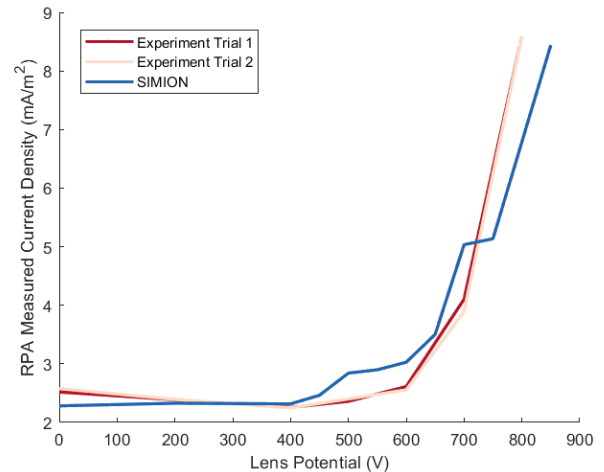


**Fig. 10:** Experimental and modeled current density measured by the RPA for varying focus lens potentials.

the RPA do not vary as the potential on the Langmuir probe varies from 0 to -100 V. This indicates that the Langmuir probe simply being in close proximity to the lens is sufficient to disturb the ion trajectories, regardless of the probe potential. Because of this, these results are presented independent of the Langmuir probe potential. The experimental results, conducted on different days, show excellent agreement with each other, indicating repeatability of this setup. The experimental and SIMION results also show good agreement. Therefore, it may reasonably be concluded that the beam is telescoped at 650 V. Furthermore, the increase in current density for potentials higher than 600 V validates that the beam is being increasingly focused. Future experiments with only the RPA may further validate these conclusions. Overall, the thin electrostatic focusing lens may be utilized to ensure a uniform flow through the experimental region of the chamber.

## V. PRELIMINARY WAKE FORMATIONS

It has been shown that the expanding and focusing lens can individually be utilized to manipulate beam parameters. However, the setup of the expanding lens requires sub-millimeter precision to avoid the beam being translated. This may be accounted for in future experiments by placing the focusing lens and spacecraft primitive on a stepper motor setup and moving them into the path of the beam. Alternatively, one lens may be utilized to enable the wake experiment, depending on whether expansion of the beam or a uniform flow is prioritized. Example lens setups and the resulting wake formations when a -100 V, 50 mm cube is placed in the wake are shown in Fig. 11. Utilizing solely the expanding lens results in the largest beam radius of 59 mm at the front of the cube. This allows for a larger distance between the edge of the cube and the beam edge, which may provide more insights into the influence of fast flowing ions on electron beam and secondary electron trajectories. Conversely, the focusing lens results in a thin sheath of ions surrounding the cube, or a radius of 31 mm at the cube front, but the wake converges before reaching

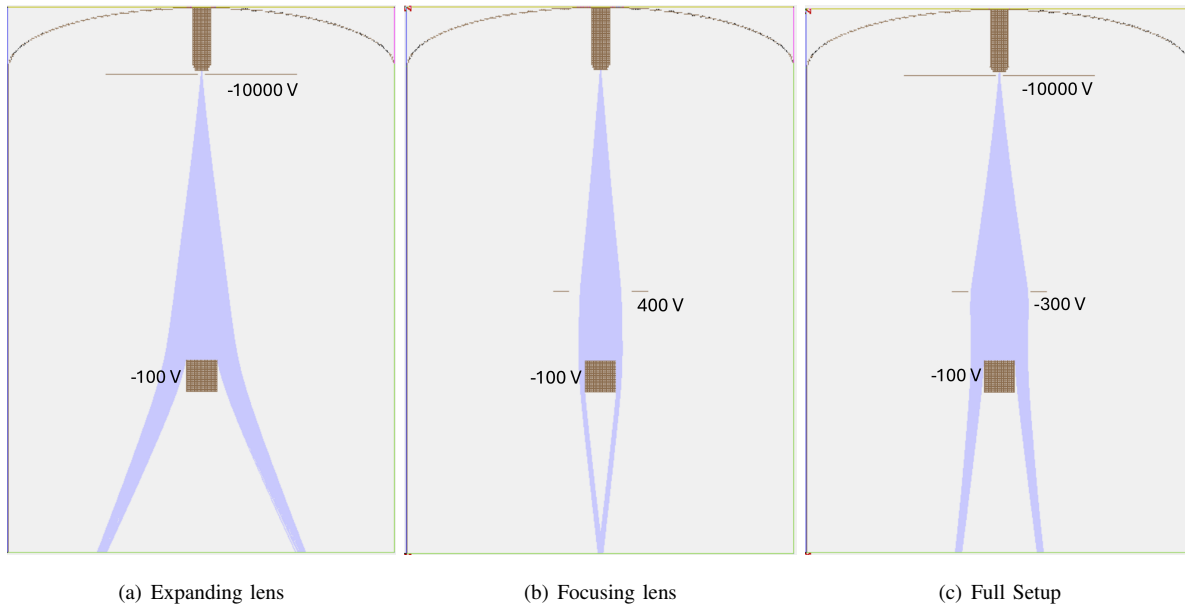


**Fig. 11:** Example lens configurations and resulting wake generation

the bottom of the chamber. This allows for better insight into a converging wake that would form in space plasma. It should also be noted that the potential of the focusing lens is decreased to account for the negative cube, as a potential of 650 V causes the ions to all impact the front or side of the cube. Finally, utilizing both lenses allows for the expansion of the wake to be minimized without sacrificing the thickness of the ion beam surrounding the cube, with a beam radius of 43 mm.

Each lens setup also results in different representative spacecraft sizes. The average ion density in the cislunar solar wind environment is  $6E6 \text{ m}^{-3}$ . Using Equations 1 and 2, the 5 cm cube represents 4.8, 9.0, and 6.6 m spacecraft in the solar wind for the expanding lens, focusing lens, and both lenses, respectively. These lengths may all reasonably represent a spacecraft diameter, so the experimental wakes generated may then reasonably represent cislunar spacecraft wake formations.

## VI. CONCLUSIONS

The installation and characterization of simple electrostatic lenses to widen and focus an ion beam is presented. The expanding lens shows good agreement with numerical simulations, and translations of the beam are found to be caused by sub-millimeter offsets of the lens. Wake experiments may be conducted despite this by placing the spacecraft primitive on a stepper motor setup and moving it into the path of the beam. Alternatively, purposefully moving the lens off-center may allow for the ion beam to impact a spot outside the original line of sight of the ion gun. The focusing lens is also shown to narrow the beam as desired, and the experimental and simulation results show good agreement. This enables the lens design to be tested numerically and reliably recreated in a vacuum chamber setup, thus speeding up experimental setup and test times.

Numerical simulations demonstrate the different types of wakes that may be generated from the same ion beam and object with various configurations of the lenses. Thus, an ion beam property of interest, such as distance between the object and beam edge, may be set and the lens designed altered to satisfy this requirement. Future work may involve implementing the expanding and focusing lens at the same time in the vacuum chamber and conducting wake experiments to validate the preliminary numerical simulations.

## ACKNOWLEDGEMENTS

This work is supported by a NASA Space Technology Graduate Research Opportunity. The authors would like to thank Leya Shaw for her help in troubleshooting and installing the electrostatic lenses.

## REFERENCES

- [1] M. Bengtson, K. Wilson, J. Hughes, and H. Schaub, "Survey of the electrostatic tractor research for reorbiting passive geo space objects," *Astrodynamics*, vol. 2, no. 4, pp. 291–305, Dec 2018.
- [2] E. A. Hogan and H. Schaub, "Impacts of tug and debris sizes on electrostatic tractor charging performance," *Advances in Space Research*, vol. 55, no. 2, pp. 630–638, January 15 2015.
- [3] —, "Impacts of hot space plasma and ion beam emission on electrostatic tractor performance," *IEEE Transactions on Plasma Science*, vol. 43, no. 9, pp. 3115–3129, Sept. 2014.
- [4] —, "Space weather influence on relative motion control using the touchless electrostatic tractor," *The Journal of the Astronautical Sciences*, vol. 63, no. 3, pp. 237–262, 2016.
- [5] M. T. Bengtson, K. T. Wilson, and H. Schaub, "Experimental results of electron method for remote spacecraft charge sensing," *Space Weather*, vol. 18, no. 3, pp. 1–12, 2020.
- [6] Álvaro Romero Calvo, J. Hammerl, and H. Schaub, "Touchless potential sensing of complex differentially-charged shapes using secondary electrons," in *AIAA SCITECH 2022 Forum*, 2022.
- [7] K. T. H. Wilson and H. Schaub, "X-ray spectroscopy for electrostatic potential and material determination of space objects," *IEEE Transactions on Plasma Science*, vol. 47, no. 8, pp. 3858–3866, Aug. 2019.
- [8] K. T. Wilson, M. T. Bengtson, and H. Schaub, "X-ray spectroscopic determination of electrostatic potential and material composition for

- spacecraft: Experimental results," *Space Weather*, vol. 18, no. 4, p. e2019SW002342, 2020.
- [9] A. Romero Calvo, K. Champion, and H. Schaub, "Enabling ultraviolet lasers for touchless spacecraft potential sensing," *IEEE Transactions on Plasma Science*, vol. 51, no. 9, pp. 2468–2481, Sept. 2023.
- [10] F. Casale, H. Schaub, and J. D. Biggs, "Lyapunov optimal touchless electrostatic detumbling of geostationary debris using surface multisphere models," *AIAA Journal of Spacecraft and Rockets*, vol. 58, no. 3, 2021.
- [11] H. Schaub and D. F. Moorer, "Geosynchronous large debris reorbiter: Challenges and prospects," *The Journal of the Astronautical Sciences*, vol. 59, no. 1, pp. 161–176, Jun 2012.
- [12] S. T. Lai, *Fundamentals of Spacecraft Charging: Spacecraft Interactions with Space Plasmas*. Princeton University Press, 2012.
- [13] J. Maxwell and H. Schaub, "Low earth orbit plasma wake shaping and applications to on-orbit proximity operations," *IEEE Transactions on Plasma Science*, vol. 47, no. 10, pp. 4760–4769, 2019.
- [14] W. Oran, U. Samir, N. H. Stone, and E. Fontheim, "Laboratory observations of electron temperature in the wake of a sphere in a streaming plasma," *Planetary and Space Science*, vol. 23, no. 7, pp. 1081–1083, 1975.
- [15] S. Raychaudhuri, J. Hill, H. Y. Chang, E. K. Tsikis, and K. E. Lonngren, "An experiment on the plasma expansion into a wake," *The Physics of Fluids*, vol. 29, no. 1, pp. 289–293, 01 1986. [Online]. Available: <https://doi.org/10.1063/1.865994>
- [16] K. Svencs and J. Trøim, "Laboratory simulation of vehicle-plasma interaction in low earth orbit," *Planetary and space science*, vol. 42, no. 1, pp. 81–94, 1994.
- [17] S. Hester and A. A. Sonin, "A laboratory study of the wakes of ionospheric satellites," *AIAA Journal*, vol. 8, no. 6, pp. 1090–1098, 1970.
- [18] C. Enloe, D. Cooke, S. Meassick, C. Chan, and M. Tautz, "Ion collection in a spacecraft wake: Laboratory simulations," *Journal of Geophysical Research: Space Physics*, vol. 98, no. A8, pp. 13 635–13 644, 1993.
- [19] R. Biasca and J. Wang, "Ion current collection in spacecraft wakes," *Physics of Plasmas*, vol. 2, no. 1, pp. 280–288, 01 1995. [Online]. Available: <https://doi.org/10.1063/1.871098>
- [20] W. Yu, J. Wang, and K. Chou, "Laboratory measurement of lunar regolith simulat surface charging in a localized plasma wake," *IEEE Transactions on Plasma Science*, vol. 43, no. 12, pp. 4175–4181, 2015.
- [21] H. Liebl, *Applied charged particle optics*. Springer, 2008, vol. 2012.
- [22] I. Drummond, "The ion optics of low-energy ion beams," *Vacuum*, vol. 34, no. 1-2, pp. 51–61, 1984.
- [23] M. Szilagyi, *Electron and ion optics*. Springer Science & Business Media, 2012.
- [24] P. Dahl, *Introduction to electron and ion optics*. Elsevier, 2012.
- [25] H. Wollnik, "Ion optics in mass spectrometers," *Journal of mass spectrometry*, vol. 34, no. 10, pp. 991–1006, 1999.
- [26] T. W. Burgoyne and G. M. Hieftje, "An introduction to ion optics for the mass spectrograph," *Mass Spectrometry Reviews*, vol. 15, no. 4, pp. 241–259, 1996.
- [27] C. Baker and R. Bingham, "Plasma lens for ion-beam focusing," in *APS Division of Plasma Physics Meeting Abstracts*, vol. 2023, 2023, pp. JO03–009.
- [28] R. Langford, A. Petford-Long, and P. Gnauck, "Focused ion beam based sample preparation techniques," *Microscopy and Microanalysis*, vol. 8, no. S02, pp. 46–47, 2002.
- [29] M. Schaffer, J. Mahamid, B. D. Engel, T. Laugks, W. Baumeister, and J. M. Plitzko, "Optimized cryo-focused ion beam sample preparation aimed at in situ structural studies of membrane proteins," *Journal of structural biology*, vol. 197, no. 2, pp. 73–82, 2017.
- [30] Y. Zhang, M. L. Crespillo, H. Xue, K. Jin, C.-H. Chen, C. L. Fontana, J. T. Graham, and W. J. Weber, "New ion beam materials laboratory for materials modification and irradiation effects research," *Nuclear Instruments and Methods in Physics Research Section B: Beam Interactions with Materials and Atoms*, vol. 338, pp. 19–30, 2014.
- [31] S. Taller, D. Woodley, E. Getto, A. M. Monterrosa, Z. Jiao, O. Toader, F. Naab, T. Kubley, S. Dwaraknath, and G. S. Was, "Multiple ion beam irradiation for the study of radiation damage in materials," *Nuclear Instruments and Methods in Physics Research Section B: Beam Interactions with Materials and Atoms*, vol. 412, pp. 1–10, 2017.
- [32] J. Maxwell, "Development of Electrostatic Actuation Techniques for Close-Proximity Formation Flying in Low Earth Orbit Plasma Wakes," Ph.D. dissertation, University of Colorado Boulder, Aug. 2020. [Online]. Available: <https://hanspeterschaub.info/Papers/grads/JordanMaxwell.pdf>
- [33] K. Champion and H. Schaub, "Feasibility of cislunar spacecraft wake generation," in *AIAA SciTech*, National Harbor, Maryland, January 23–28 2023.
- [34] C. J. Capon, M. Brown, and R. R. Boyce, "Scaling of plasma-body interactions in low earth orbit," *Physics of Plasmas*, vol. 24, no. 4, p. 042901, 2017. [Online]. Available: <https://doi.org/10.1063/1.4979191>
- [35] F. B. Leahy, "Sls-spec-159, cross-program design specification for natural environments (dsne)," National Aeronautics and Space Administration, Tech. Rep., 2021.
- [36] P. Li, N. Hershkowitz, and G. Severn, "Building langmuir probes and emissive probes for plasma potential measurements in low pressure, low temperature plasmas," *JOVE (Journal of Visualized Experiments)*, no. 171, p. e61804, 2021.
- [37] F. F. Chen, "Langmuir probe diagnostics," in *IEEE-ICOPS Meeting, Jeju, Korea*, vol. 2, no. 6. Citeseer, 2003.
- [38] R. B. Lobbia and B. E. Beal, "Recommended practice for use of langmuir probes in electric propulsion testing," *Journal of Propulsion and Power*, vol. 33, no. 3, pp. 566–581, 2017.